Eur Biophys J (2010) 39:1057–1068
DOI 10.1007/s00249-009-0451-z

ORIGINAL PAPER

Salt bridges in the miniature viral channel Kcv are important for function

Brigitte Hertel · Sascha Tayefeh · Thomas Kloss · Jennifer Hewing · Manuela Gebhardt · Dirk Baumeister · Anna Moroni · Gerhard Thiel · Stefan M. Kast

Received: 30 January 2009 / Revised: 14 March 2009 / Accepted: 31 March 2009 / Published online: 24 April 2009

Abstract The viral potassium channel Kcv comprises only 94 amino acids, which represent the pore module of more complex K^+ channels. As for Kir-type channels, Kcv also has a short N-terminal helix exposed to the cytoplasm, upstream of the first transmembrane domain. Here we show that this helix is relevant for Kcv function. The presence of charged amino acids, which form dynamic inter- and intra-subunit salt bridges is crucial. Electrophysiological measurements, yeast rescue experiments and molecular dynamics simulations show that mutants in which the critical salt bridge formation is impaired have no or reduced channel activity. We conclude that these salt bridges destabilise the complexation of K^+ ions by negative charges on the inner transmembrane domain at the entrance into the cavity. This feature facilitates a continuous and coordinated transfer of ions between the cavity and the cytoplasm for channels without the canonical bundle crossing.

Keywords Salt bridge · Kcv-channel · Channel gating · K^+ channel · MD simulation

List of abbreviations

TM	Transmembrane
GFP	Green fluorescent protein
MD	Molecular dynamic

Introduction

Channels are membrane-spanning proteins, which enable a rapid transfer of ions across biological membranes. Their physiological role is characterised by two functional features, selectivity and gating (Hille 1992). Selectivity describes the ability of a channel protein to efficiently discriminate between ions, e.g. between K^+ and Na^+. Gating means that the channel protein fluctuates stochastically between open and closed conformations; ion flow is possible only in the open state. Many relevant physiological control factors affect the transition between these two states, and in this way they are able to modulate channel activity.

Recent advances in structural biology have provided detailed insights into the architecture of ion channels (Doyle et al. 1998; Kuo et al. 2003; MacKinnon 2003; Shi et al. 2006). In combination with computational methods (Roux et al. 2004; Khalili-Araghi et al. 2006; Roux and Schulten 2004; Domene et al. 2003), these are now providing an increasingly sharper picture on the mechanisms that drive relevant conformational changes in the proteins. In this context, salt bridges, which stochastically form and break between different domains, emerge as important mechanism for intramolecular interactions (Beckstein et al. 2003). In the bacterial channel, for example OmpA, it was highlighted that stochastic formation of alternative salt

Viral membrane proteins, Heidelberg, December 2008.

B. Hertel · S. Tayefeh · J. Hewing · M. Gebhardt · D. Baumeister · G. Thiel (✉)
Institute for Botany, TU-Darmstadt,
Schnittspahnstrasse 3-5, 64287 Darmstadt, Germany
e-mail: thiel@bio.tu-darmstadt.de

S. Tayefeh · T. Kloss · S. M. Kast
Eduard-Zintl-Institut für Anorganische
und Physikalische Chemie, TU-Darmstadt,
Petersenstrasse 20, 64287 Darmstadt, Germany

A. Moroni
Department of General Physiology and Biochemistry,
Università degli Studi di Milano, Milan, Italy

bridges result either in an occlusion or opening of the ion pathway; salt bridge dynamics may hence explain the molecular mechanism of gating in this channel (Hong et al. 2006; Moroni and Thiel 2006). In the inward rectifying K^+ channels, HCN1 and CNGA1 salt bridges form between the c-linkers of neighbouring subunits as well as between a c-linker and the cyclic-nucleotide binding site within a monomer (Craven and Zagotta 2004). The fact that experimental disruption of these salt bridges augments channel open probability suggests that they tend to stabilise a closed conformation and implies their involvement in gating. Also in the pore of K^+ channels salt bridges seem to play a role in channel gating: in KcsA interaction between residues Glu71 and Asp80 promotes conformational changes in the filter that presumably abrogates conductance. Disrupting this salt bridge, like in the 71A mutant results in a channel, which shows no more inactivation (Cordero-Morales et al. 2007).

Recently we investigated structure/function correlates in the miniature viral K^+ channel Kcv. This channel has the hallmarks of complex K^+ channels, but has the special advantage of viral proteins that the monomer, 94 aa, is truly minimal (Plugge et al. 2000) and consists of two transmembrane (TM) domains, a pore loop with the canonical selectivity filter minimal N and no cytosolic C terminus; like other K^+ channels it forms a tetramer (Plugge et al. 2000; Pagliuca et al. 2007; Tayefeh et al. 2009).

Structural predictions and molecular dynamics (MD) simulations (Gazzarrini et al. 2004; Tayefeh et al. 2007, 2009) confirm that the inner helices are too short to form a structural barrier, the so-called bundle crossing, at the cytosolic side of the pore cavity. This structure is considered the main gate in KcsA and needs to be removed by a pH-driven conformational change in order to allow ion flow through the pore. In the case of Kcv, ions should therefore be free to enter or leave the cavity without a conformational change (Jiang et al. 2002; Alam and Jiang 2009). This is indeed the case, as has been seen in MD simulations of both a truncated KirBac1.1 model (a "functional analogue") that matches the Kcv sequence (Kuo et al. 2003; Tayefeh et al. 2007) as well as a Kcv homology model after extensive MD refinement (Tayefeh et al. 2009). Computational modelling showed that the viral channel exhibits distinct salt bridge patterns at the intracellular entrance to the cavity, which seems to control exchange between cavity and cytosolic solution (Tayefeh et al. 2007). Ion exchange is governed by transient K^+ binding to negatively charged C-terminal carboxyl groups, which switch back and forth between salt bridge partners in the protein and K^+ ions in a "turnstile" manner. It could be shown for the KirBac1.1-Kcv model (Tayefeh et al. 2007) that disruption of C/N-terminal salt bridges results in very strong ion binding to the C-terminus, which promotes a K^+ block at the mouth preventing further ion exchange. The intramolecular interaction in this domain of the channel is not confined to the viral channel Kcv. A similar pattern is found in the NaK channel (Shi et al. 2006) suggesting that these salt bridge patterns play a more general role in channel function.

In the present work we substantiate the view that salt bridges are crucial for channel function by combining experimental and computational approaches. We analyse the effect of truncation and point mutations in the intracellular mouth region that influence salt bridge formation. Experimental results are interpreted by theoretical illustration of the microscopic scenario. The computational model is evaluated by further experimental tests of theoretical predictions. This hybrid strategy leads to a coherent picture of the salt bridge effects.

Materials and methods

Mutageneses and transfection of mammalian cell lines

The Kcv gene was cloned in frame into the BglII and EcoRI sites of the pEGFP-N2 eukaryotic expression vector (Clontech) upstream of the EGFP gene with deletion of the Kcv stop codon. The mutant channels with truncations in the N-terminus (ΔN-Kcv) were constructed by standard PCR techniques by deletion of the first 3, 7, 8, 9 or 11 aa and inserted into the pEGFP-N2 vector upstream of the GFP gene as described above. The products were validated by sequencing. Point mutations were created by the QuikChange method (Stratagene) and confirmed by sequencing the DNA insert. For functional expression the chimeras of Kcv and GFP (Kcv:GFP) and the Kcv-mutants were transfected with 1.5 μg DNA into human HEK293 cells. The plasmid pEGFP-N2 containing the GFP gene only was used for mock transfection of control cells. HEK293 cells were transiently transfected using the liposomal transfection reagent metafectene (Biontex).

Electrophysiology

Experiments were performed on HEK293 cells incubated after transfection at 37°C in 5% CO_2 for 2–3 days. On the day before the experiment, cells were dispersed by trypsin, plated at a low density on 35 mm culture dishes and allowed to settle over night. Dishes were then placed on the stage of an inverted microscope and single cells patch-clamped in the whole-cell configuration according to standard methods (Hamill et al. 1981) using an EPC-9 Patch Clamp amplifier (HEKA, Lambrecht, Germany). Data acquisition and analysis were performed using Pulse software (HEKA).

Cells were perfused by room temperature with a control solution containing: 100 mM KCl, 1.8 mM $CaCl_2$, 1 mM $MgCl_2$, 5 mM HEPES (pH 7,4). Choline-Cl was used to adjust the osmolarity to 300 mOsmol. Fast delivery of the solution was obtained by means of a perfusion pipette positioned on top of the cell under study, which allowed relatively rapid solution changes. Whole-cell pipettes contained: 130 mM D-potassium-gluconic acid, 10 mM NaCl, 5 mM Hepes, 0.1 mM GTP (Na salt), 0.1 μM $CaCl_2$, 2 mM $MgCl_2$, 5 mM Phosphocreatine, 2 mM ATP (Na salt) (pH 7.4). Currents were measured in the whole cell configuration; cells were clamped from a holding voltage (0 mV) to test voltages between +60 and −160 mV.

Saccharomyces cerevisiae complementation assays

Selection experiments were performed as reported previously (Balss et al. 2008). Viral K^+ channels or their mutants were transformed into SGY1528 yeast strain (*Mat a ade*2–1 *can*1–100 *his*3–11,15 *leu*2–3,112 *trp*1–1 *ura*3–1 *trk*1:HIS3 *trk*2:TRP1), which are deficient in endogenous K^+ uptake systems. Yeasts from the same stock were grown in parallel under nonselective conditions on plates containing 100 mM KCl and on selective conditions on agar containing 1 or 0.5 mM KCl. Growth experiments were done at 30°C.

Image analysis

The co-localisation analysis is based on confocal images showing the plane of HEK293 cells. Images were acquired with a Leica SP confocal system equipped with a 63x Apo plan water objective was used. Green fluorescence (GFP, ER-Tracker™ Green (BODIPY® FL glibenclamide, Invitrogen)) was excited by a 488-nm laser line and detected in the range from 505 to 540 nm, while ER-Tracker™ Red (BODIPY® FL glibenclamide, Invitrogen) was excited by a 543-nm laser line and detected from 590 to 650 nm. Three-fold averaging was applied during data acquisition in both detection channels to reduce unspecific signal. Before analysis the microscopic pictures were background reduced to a level of 0 outside the cells. By using the JACoP plugin of imageJ the pairs of pictures were analysed using Pearson's and Li's algorithms (Bolte and Cordelières 2007).

Molecular dynamics simulations

MD simulation data for Kcv wild-type (wt) was taken from earlier work (Tayefeh et al. 2009) for further analysis. Additionally, we constructed homology models for ΔN8-Kcv and ΔN14-Kcv based on the alignment shown in Fig. 1 using Modeller V8.1 (Marti-Renom et al. 2000). The resulting 3D structures were embedded in a DMPC lipid bilayer and solvated in aqueous KCl solution, following closely the procedures presented in earlier work (Tayefeh et al. 2007, 2009). We placed 64 lipid molecules on the intracellular and 54 on the extracellular side initially in a periodic box of 72 Å × 72 Å × 92 Å. The total ion number was (K^+/Cl^-) 19/19 for ΔN8-Kcv and 19/19 for ΔN14-Kcv. The total number of atoms was 48,805/48,683 including 9,663/9,761 water molecules for the ΔN8-Kcv and the ΔN14-Kcv system, respectively. The simulations were performed using all-atom potential energy functions CHARMM22 for proteins (MacKerell et al. 1998) and CHARMM27 for phospholipids (Schlenkrich et al. 1996) with the NAMD2.6 molecular dynamics package (Kale et al. 1999). The Lennard-Jones interactions were calculated with a smooth cutoff over a distance of 10–12 Å. Production runs in the *NpT* ensemble were performed at $T = 330$ K and $p = 1$ atm using an integration time step of 2 fs and constrained distances between hydrogen and heavy atoms. Electrostatic interactions forces were treated by the smooth particle mesh Ewald algorithm (Essmann et al. 1995) at a grid resolution of ca. 1 Å. Restraints on the filter atoms were initially applied and lifted later. The total simulation time was 102 ns for ΔN8-Kcv and 99 ns for ΔN14-Kcv. As a measure of conformational stability, we computed the root

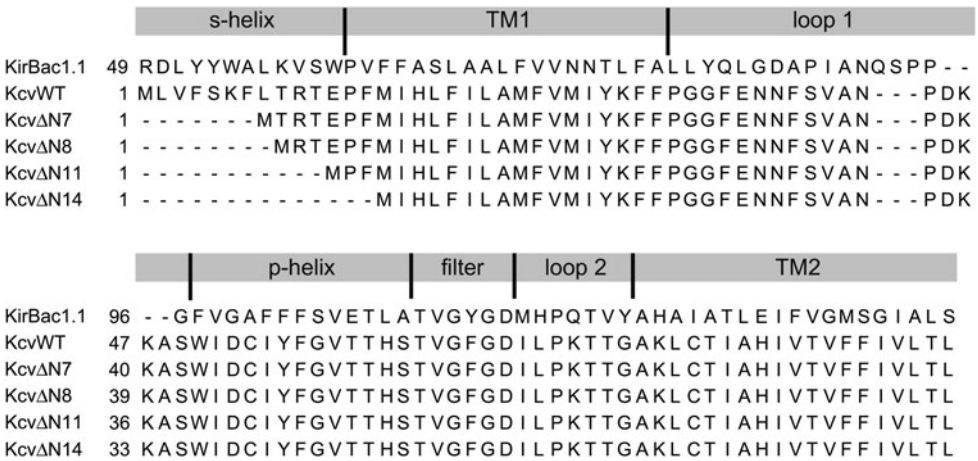

Fig. 1 Alignment of KirBac1.1 with Kcv wild-type and several representative truncation mutants. *s-helix* N-terminal slide-helix; *TM* transmembrane domain; *p-helix* pore helix; *filter* selectivity filter; *loop* turret loop region

mean-square deviation (RMSD) of Cα atoms from the starting structure which never exceeded 5 Å in any of our simulations.

Data analysis

Following earlier work (Tayefeh et al. 2007, 2009), average structures were extracted by a mean-field simulated annealing approach. Average distances were calculated from the simulations with restrained filter atoms, which enter a harmonic site–site distance restraining potential as reference values. Restraint force constants were set to 10 kcal mol^{-1} $Å^{-1}$ for all Cα-Cα pairs, and to 0.20 (ΔN8-Kcv)/0.25 kcal mol^{-1} $Å^{-1}$ (ΔN14-Kcv) for all other heavy atom distances within a range of 11 Å, weighted by the inverse fluctuation of the target distance. The resulting average structures were subjected to 3D RISM (reference interaction site model) calculations (Beglov and Roux 1997; Kovalenko and Hirata 1998), using methodology described previously (Tayefeh et al. 2007). In short, the theory predicts the local ionic density on a spatial 3D grid around the channel protein, given the bulk concentration and temperature as input. Locally high density corresponds to regions of strong ion attraction. The density is directly related to the free energy surface governing single ion transport. 3D RISM results were obtained for Kcv-wt, and the two truncation mutants dissolved in 1 M KCl solution at a temperature of 298.15 K.

Results and discussion

The Kcv channel requires a minimal length of the cytoplasmic N-terminus

In a previous study, we have shown that complete removal of the first 14 amino acids (Leu^2-Met^{15}) of the N-terminus of Kcv renders the channel inactive (Moroni et al. 2002; Gazzarrini et al. 2002). The failure to detect a Kcv-specific current could not be explained by an impaired synthesis of the channel protein (Moroni et al. 2002). To study further the functional significance of the N-terminus we sequentially truncated it. The respective mutants were expressed in HEK293 cells and monitored for function. Figure 2a shows the current responses of a HEK293 cell mock-transfected with GFP (control) to a standard pulse protocol (see "Materials and methods"). These cells show the typical background conductance of HEK293 cells with a low conductance at negative clamp voltages and a small K^+ outward rectifier at positive voltages (Fig. 2a, e). In the control cells, the ratio of cord conductance at negative voltages (−20 to −60 mV, G_{neg}) versus conductance at positive voltages (0 to +60 mV, G_{pos}) was always less than 1 (0.43 + 0.12, $n = 27$). In contrast, when cells are transfected with a chimera of Kcv and GFP (Kcv:GFP), they frequently show a large inward current with typical features. An example of this current and the corresponding current/voltage (I/V) relation is shown in Fig. 2b, e. In this case, the conductance increases linearly with clamp voltage between 0 and about −80 mV; at more negative voltages, the conductance passes a maximum. It has been shown that this pronounced inward current, which saturates at voltages more negative of about −100 mV in HEK293 cells is due to the activity of the Kcv:GFP channel (Moroni et al. 2002; Hertel et al. 2006). In comparison to mock-transfected control cells, the ratio of G_{neg}/G_{pos} in cells with clear cut Kcv conductance is always larger than 1 (1.4 ± 0.4, $n = 27$). The distinct difference in the G_{neg}/G_{pos} ratio between cells without and with appreciable Kcv type conductance prompted us to use the parameter $G_{neg}/G_{pos} \geq 1$ as an estimate for the fractional detection of Kcv type channel activity.[1] According to this criterion, it happens that about 65% in GFP fluorescent HEK293 cells reveal this type of conductance (Fig. 2f). In the following, we use this value of fractional detection as a measure for quantifying functional mutants with respect to the Kcv-wt channel.

Shortening of the N-terminus by three (ΔN3-Kcv:GFP) and seven (ΔN7-Kcv:GFP) amino acids had no appreciable effect neither on the fractional detection (Fig. 2c, f) nor on the characteristics of the Kcv conductance. Figure 2c reports the current response of a HEK293 cell transfected with ΔN7-Kcv:GFP. The current reveals the same features as the current conducted by the wild type channel (Fig. 2e). Also the fractional detection was not reduced compared to that of the full-length channel (Fig. 2f). Further tests revealed that this current exhibited a similar degree of selectivity for K^+ over Na^+ as the full-length channel. Also the sensitivity to Ba^{2+}, a Kcv channel blocker (Plugge et al. 2000), was not affected (data not shown).

Any further shortening of the N-terminus caused a dramatic decrease of fractional detection. Only one out of 19 cells transfected with ΔN8-Kcv:GFP revealed a conductance with the features of Kcv:GFP. The ΔN8-Kcv:GFP mutant appears to be the critical transition for the detection of functional channels; mutants in which the N-terminus was further truncated (ΔN9-Kcv:GFP, ΔN11-Kcv:GFP) never revealed an appreciable Kcv like conductance (Fig. 2d, f).

[1] It should be noted that by the choice of this threshold the presence of the viral channel in the plasma membrane might be underestimated if Kcv currents are small compared to the background. The procedure was nonetheless chosen because it allows a clear-cut separation of the Kcv conductance from the background current.

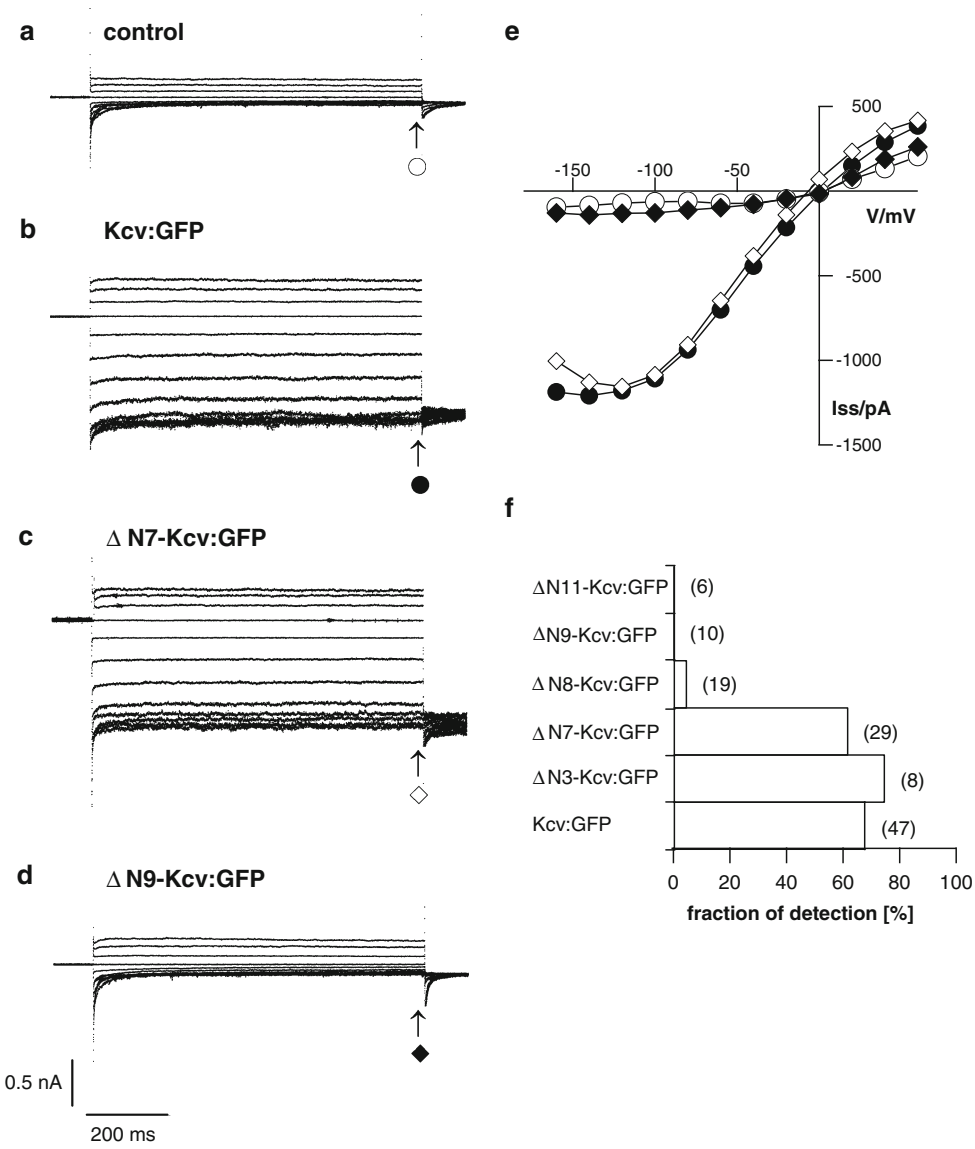

Fig. 2 Shortening of the Kcv-N-terminus beyond a critical length renders the channel inactive. **a**–**d** Current responses of HEK293 cells transfected with GFP (**a**), Kcv:GFP (**b**) and channels in which the first seven (ΔN7-Kcv:GFP) (**c**) or the first nine amino acids (ΔN9-Kcv:GFP) (**d**) were truncated. Currents were measured in whole cell configuration from cells in bath with 100 mM K^+ to standard voltage protocol from holding voltage (0 mV) to test voltages between +60 and −160 mV. **e** Steady-state I/V relation of currents in **a**–**d**; symbols cross-reference with symbols at current traces. **f** Fractional detection of Kcv:GFP and mutants in HEK293 cells. Number of recordings in **f** is indicated in *parentheses*

Truncation of N-terminus does not impair sorting into the secretory pathway

The failure to detect activity of the truncated Kcv mutants in HEK cells could, in principle, be not only due to impaired function but also due to an interruption in any step between protein synthesis and trafficking to the plasma membrane. We can exclude the possibility that mutations affected protein synthesis; all channel mutants were produced in HEK293 cells and judging from the GFP distribution they were all associated with membrane structures in the cells (e.g. Moroni et al. 2002). In a previous study, however, we found that modifications of a viral K^+ channel could result in an altered sorting (Balss et al. 2008). To monitor sorting of the truncated channel in comparison to the wild type (wt) channel, we examined the targeting into the secretory pathway. This was achieved by measuring co-localisation of the GFP-tagged protein with the endoplasmic reticulum. In order to calibrate the system, we first labelled the ER in HEK293 cells with ER-tracker green and ER-tracker red. Typical images are shown in Fig. 3a. The expected co-localisation is illustrated in the right panel by a superposition of the green and red channel. The quantitative analysis of co-localisation is summarised by the bars on the right with a Pearson's coefficient, P, of 0.86 ± 0.06 and an intensity correlation coefficient, Ic, of 0.44 ± 0.02 ($n = 6$). These two values provide the reference for an ideal co-localisation in these images. To estimate the lower end of the scale, i.e. unspecific co-localisation, we expressed the GFP-tagged Kesv channel and stained the endoplasmic reticulum with ER-tracker red (Fig. 3b). Kesv, which does not enter the secretory pathway and is sorted into the mitochondria (Balss et al. 2008), reveals in the same experiments only a P value of 0.4 ± 0.1 and an Ic of 0.25 ± 0.04 ($n = 6$).

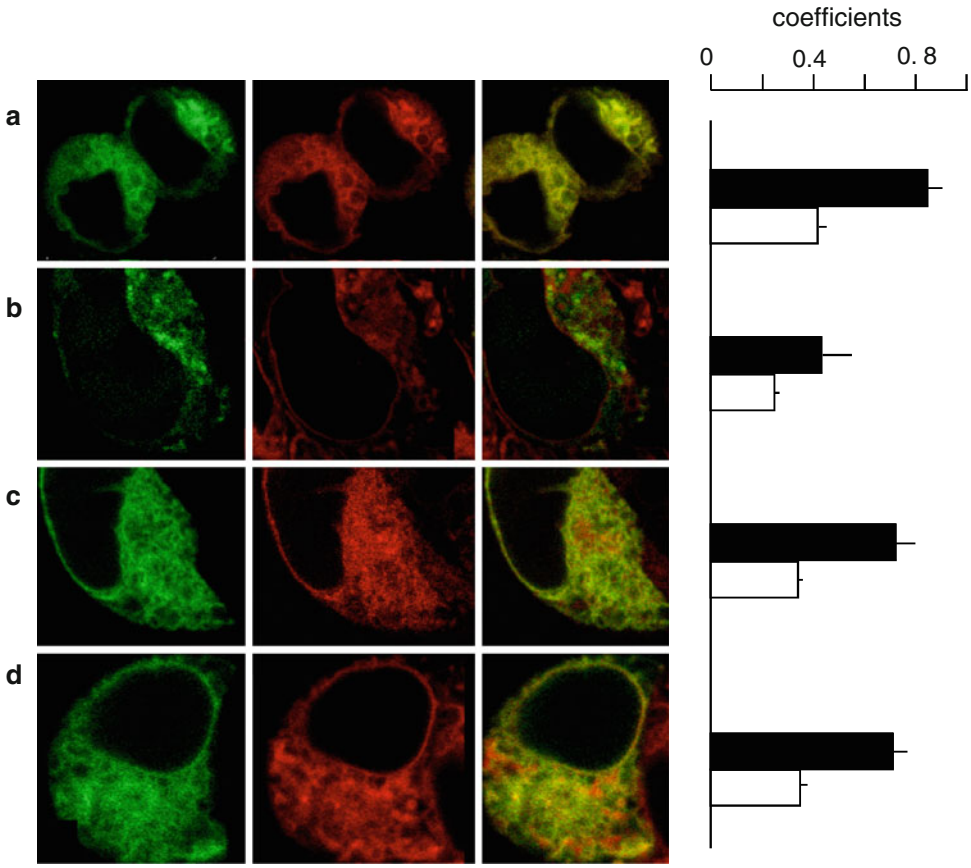

Fig. 3 The active channel Kcv:GFP and the inactive truncated channel D11-Kesv:GFP both enter the secretory pathway in HEK293 cells. **a** Confocal images of exemplary HEK293 cells stained with ER-tracker *red* (*green channel*, *image on left*) and ER-tracker *green* (*red channel*, *central*). Overlay of the two images in which co-localisation of the two colours is shown in *yellow* (*image on right*). The *bars on the right* summarise Pearson's coefficients (*P*; *solid bars*) and intensity correlation coefficients (Ic; *open bars*) from ≥6 images. **b**–**d** Same analysis as in **a** for cells **(b)** expressing Kesv:GFP (*green channel*) and with ER stained with ER-tracker *red* (*red channel*) **(c)**, expressing Kcv:GFP (*green channel*) and with ER stained with ER-tracker *red* (*red channel*) **(d)** expressing Δ11 N-Kcv:GFP (*green channel*) and with ER stained with ER-tracker *red* (*red channel*)

In the next step, Kcv:GFP or ΔN11-Kcv:GFP (a representative of the mutants, which are not detectable) were expressed in HEK293 cells, and the co-localisation with ER-tracker red analysed with the same procedure. The typical images and mean co-localisation coefficients in Fig. 3c, d show that ΔN11-Kcv:GFP is properly synthesised similar to Kcv-wt. The co-localisation analysis provides a value $P = 0.72 \pm 0.08$ and $Ic = 0.33 \pm 0.3$ ($n = 10$) for the wt channel. The values for the truncated mutant are indistinguishable from the wild type channel with $P = 0.72 \pm 0.02$ and $Ic = 0.30 \pm 0.2$ ($n = 8$) for the mutant. The results of these experiments suggest that a modification of the N-terminus of Kcv is not critical for the initial sorting; the protein is properly entering the endoplasmic reticulum and the secretory pathway and may hence finally reach the plasma membrane. The results of these experiments are not a final proof for a correct insertion of the channel protein into the plasma membrane; nonetheless, the data imply that the failure of detecting currents of some Kcv mutants is most likely due to a modification of function of the channel rather than in an impaired synthesis and sorting.

The N-terminus requires amino acids as salt bridge partners

The results from sequential truncation of the N-terminus suggest that either the length of the remaining N-terminus is critical or that the specific character of the amino acids in these positions is crucial for detecting functional channels. To address this question, we constructed mutants of ΔN7-Kcv:GFP in which the aa Thr^9 was replaced by either Ala, Ser or Asp. A test of functional expression HEK293 cells revealed that Thr^9 is not essential in this position. Mutants with Ala or Ser produce essentially the same value of fractional detection as ΔN7-Kcv:GFP. Figure 4 illustrates representative current responses and I/V relations of HEK293 cells expressing ΔN7-Kcv:GFP (Fig. 4a) or ΔN7-Kcv-T9S:GFP (Fig. 4b) with the corresponding I/V relations (Fig. 4e). The I/V relations and the fractional detection (Fig. 4e, f) of the wt- and mutant-channels are essentially the same. The same fractional detections (Fig. 4f) and I/V relations (data not shown) between wt- and mutant-channels were obtained with ΔN7-Kcv-T9A:GFP. While the protein tolerates mutations of Thr^9 into a neutral amino acid, it is strongly affected by a negatively charged aa in this region. When Thr^9 was exchanged by the negatively charged amino acid Asp cells still revealed Kcv-type currents with the typical I/V characteristics (Fig. 4c, e), but the fractional detection decreased from about 70 to 10% (Fig. 4f).

The functional assay used so far relies on recording the conductance of a chimeric channel in which Kcv is fused at the C-terminus with a GFP. To test whether the presence of

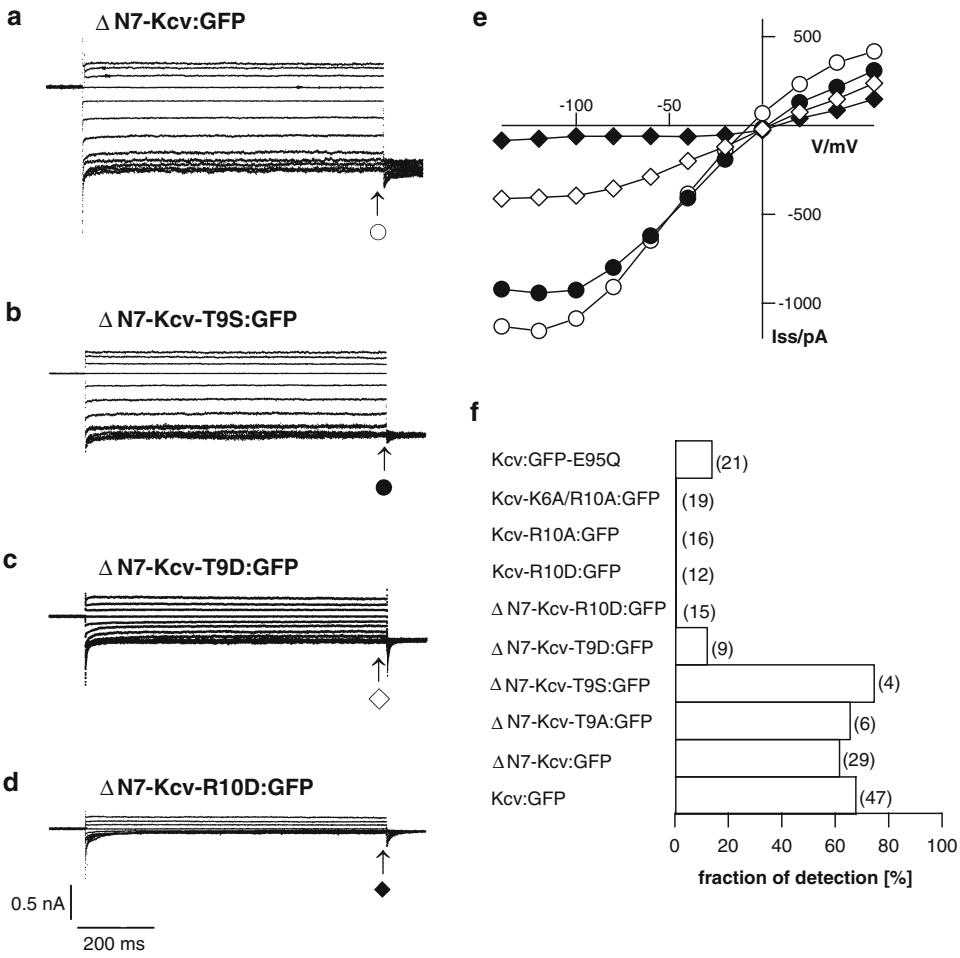

Fig. 4 Kcv channel activity is sensitive to charge patterns in C- and N-terminus. **a**–**c** Current responses of HEK293 cells transfected with ΔN7-Kcv:GFP **(a)**, ΔN7-Kcv-T9S:GFP **(b)**, ΔN7-Kcv-T9D:GFP **(c)** and ΔN7-Kcv-R10D:GFP **(d)**. Currents were measured as in Fig. 2. **e** Steady state I/V relation of currents in **a**–**d**; symbols cross-reference with symbols at current traces. **f** Fractional detection of Kcv:GFP and mutants in HEK293 cells. Number of recordings is indicated in *parentheses*

the GFP affects the sensitivity of Kcv to the length of the N-terminus, we employed yeast rescue experiments with full length Kcv, ΔN11-Kcv and ΔN8-Kcv, without GFP fusion. The assay is based on the fact that yeast mutants (Δtrk1, Δtrk2) are deprived of their endogenous K^+ uptake systems, and hence are not able to grow in low K^+ medium (Anderson et al. 1992); they only survive in a medium with high K^+ concentrations (Fig. 5, left row 100 mM K^+). When these mutants are transformed with the gene of a functional K^+ transporter, in this case Kcv, they regain the ability to grow in medium with low (0.5 and 1 mM) K^+ concentrations (Fig. 5) (Balss et al. 2008). However, when the yeast mutants are transformed with ΔN11-Kcv, they did neither grow in 0.5 mM nor in 1 mM K^+ (Fig. 5). Transformation of cells with ΔN8-Kcv is able to rescue yeast to grow in 1 mM K^+ medium but not in the lower 0.5 mM condition (Fig. 5). The results of these experiments are consistent with the HEK293 cell assay, where ΔN11-Kcv mutant had no appreciable fractional detection and the ΔN8-Kcv mutant had a reduced fractional detection compared to Kcv-wt.

Since qualitatively similar results have been obtained with Kcv constructs with and without GFP, we can conclude that Kcv function is modulated by the N-terminus; this sensitivity is not affected by the presence of the C-terminal GFP tag. Furthermore the results indicate that the first seven amino acids in the N-terminal domain are not essential for channel function. Functionality of the channel with or without a C-terminal GFP tag requires a minimal length of the N-terminal domain, which tolerates to some extent exchanges of amino acids.

Comparison of simulation models for active and inactive mutants

The average structures that result from the annealing procedure are shown in Fig. 6, where typical salt bridge patterns are emphasised. A salt bridge is defined as a close contact between unlike charges in titratable residues and/or the terminal carboxyl/amino groups. All potential salt bridge partners in the C/N-terminal region are shown explicitly in Fig. 6. For Kcv-wt and ΔN8-Kcv, a number of intra- and inter-subunit salt bridge contacts can be made which all occur during the simulation time. For the wild-type the most stable one is found between Lys^6 (positively charged side chain) and the terminal negative charge on the

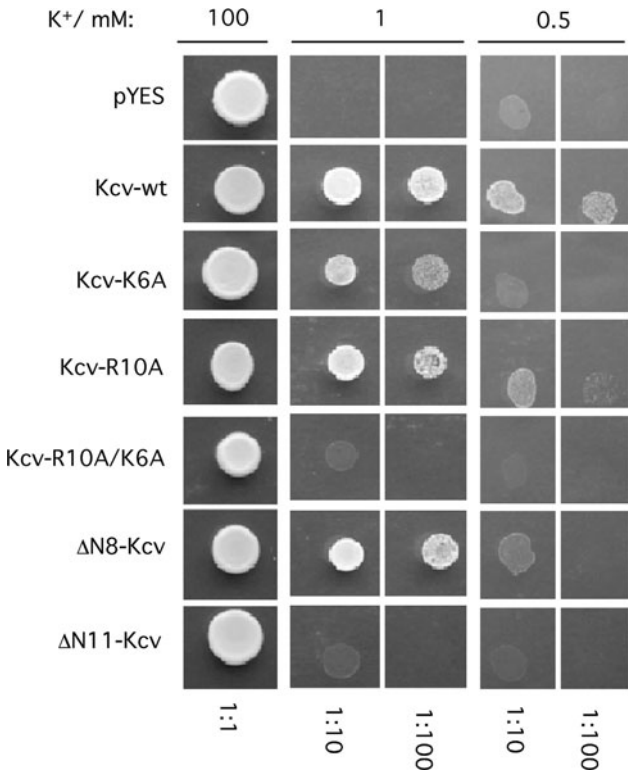

Fig. 5 Growth phenotype of yeast Δ*trk1* Δ*trk2* mutants transformed with the empty yeast shuttle vector pYES2, Kcv-wt and different Kcv channel mutants. Yeast cells were transformed with genes indicated and grown on media containing either 100 mM K^+ (*left row*) 1 mM K^+ (*central row*) and 0.5 mM K^+ (*right row*). Yeast transformed with only vector, Kcv-R10A/K6A and ΔN11-Kcv failed to complement growth in 0.5 and 1 mM K^+. The dilution of yeast on growth plates is shown below

carboxyl group of Leu^{94}. Leu^{94} (note that the numbering changes for the truncated mutants) is typically involved in the dynamic bridge making and breaking and, at the same time, transiently complexes K^+ ion. The patterns and the ion dynamics are very similar to the behaviour found earlier for the hybrid KirBac1.1-Kcv model (Tayefeh et al. 2007). The experimentally inactive ΔN14-Kcv mutant lacks the possibility to form salt bridges except between Leu^{80} (corresponding to Leu^{94} in Kcv-wt) and Met^1 which rarely occur. The negative charge on the carboxyl group of the terminal leucine is therefore more frequently exposed to the solvent as compared to the wild type and the other mutant. For the "borderline" mutant ΔN8-Kcv the probability to find the terminal Leu^{86} involved in salt bridges is lower compared with Kcv-wt and higher compared with ΔN14-Kcv.

The structural and functional implications of the differing salt bridge patterns are illustrated in Fig. 7. The diameter of the intracellular mouth of both ΔN8-Kcv and ΔN14-Kcv is smaller compared with the wild type which could be related to a reduced activity as a consequence of less frequent K^+ exchange between bulk solution and the cavity. Furthermore, as shown on the left side of Fig. 7, only Kcv-wt is capable of single-file motion through the filter and ion translocation over the entire pore length, if the filter is fully flexible. A single-file event, characterised by the concerted motion of three adjacent filter ions, is seen at around 38 ns in Fig. 7b. A cavity ion (red line) enters the innermost filter binding site, followed by an expulsion of the outmost ion to the extracellular solution and concerted upward shift of the central ion that stays in the filter (see also Tayefeh et al. 2009). All 3D RISM density distribution images are compatible with the ion dynamics analyses. The density distribution close to the intracellular mouth of ΔN14-Kcv is particularly instructive, since it illustrates, visualised as very large local density, the formation of a potassium block due to the solvent-exposed terminal Leu^{80} carboxyl groups, again very similar to the truncated

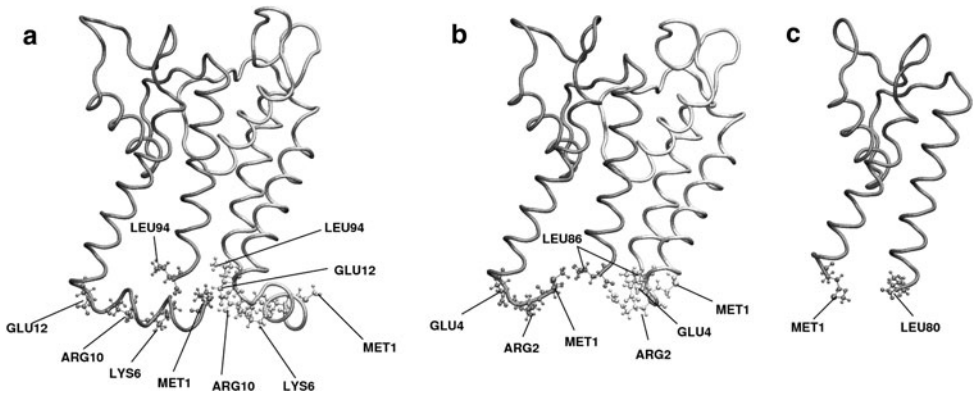

Fig. 6 Salt bridge patterns in the C/N-terminal region for average Kcv structures: Kcv wild-type (**a**), ΔN8-Kcv (**b**) and ΔN14-Kcv (**c**). The protein backbone is shown in cartoon representation, visualised by VMD (Humphrey et al. 1996). Successive truncation leads to a gradual loss of possible salt bridge partners. In **a** and **b**, two neighbouring subunits are shown since salt bridges can form within and/or between monomers

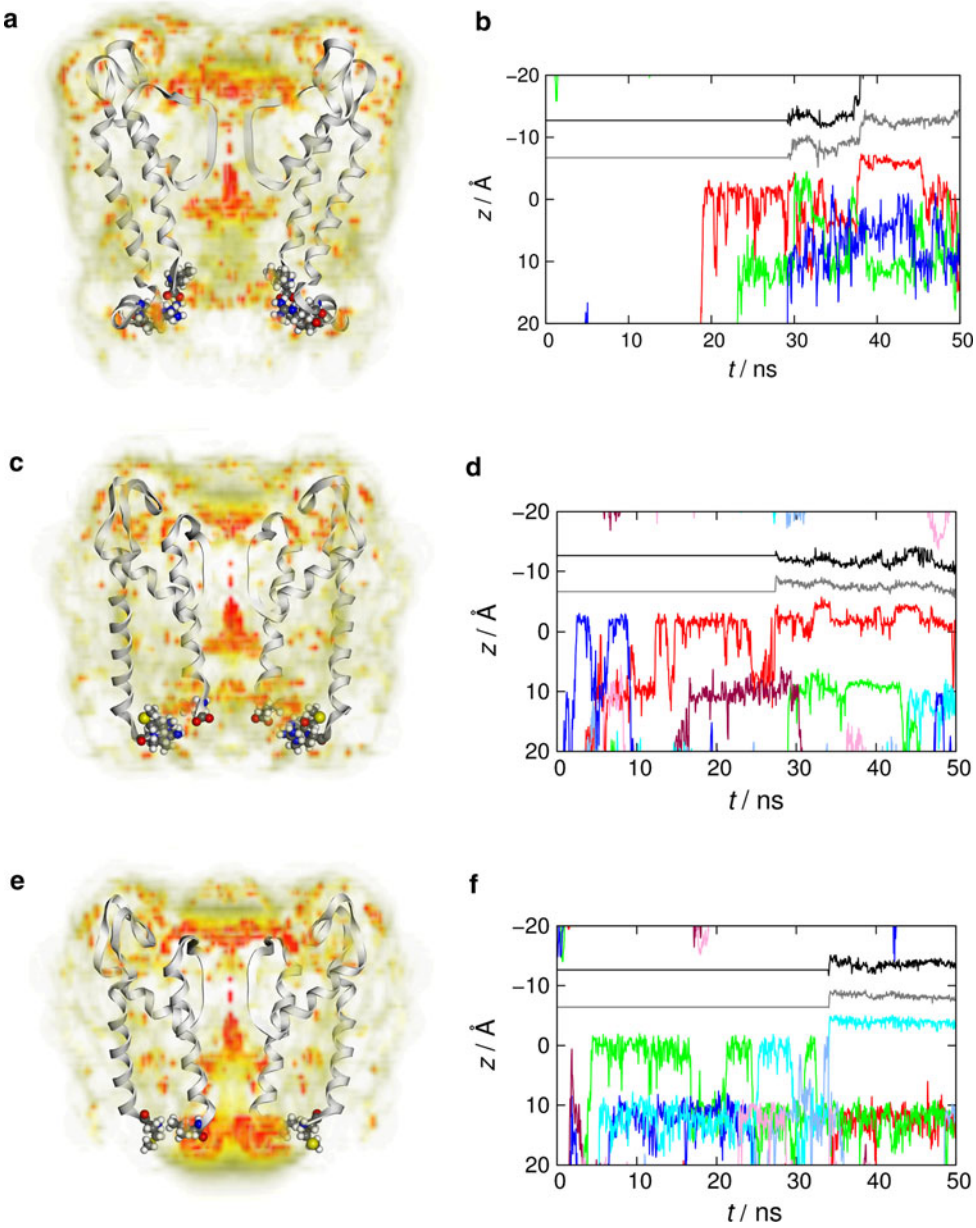

Fig. 7 K^+ density distributions from 3D RISM calculations for average channel structures in 1 M KCl solution (*left column*); *z* coordinates (along the channel axis) of K^+ ions versus MD simulation time (*right column*) for Kcv wild-type (**a**, **b**), ΔN8-Kcv (**c**, **d**) and ΔN14-Kcv (**e**, **f**). **b** Coloured version of a similar image shown in Tayefeh et al.(2009). Ion densities are colour-coded and increase from *grey* over transparent to *yellow* and *red*, visualised by MOLCAD (Brickmann et al. 1995). Only two opposing subunits are shown in ribbon representation for clarity (**a**, **c**, **e**), charged C and N-terminal residues are depicted explicitly. The dynamics (**b**, **d**, **f**) is shown for those ions only which remain within a 10-Å margin around the protein on both the cytosolic and the extracellular side for more than 200 ps; *colours* indicate different K^+ ions

KirBac1.1-Kcv model (Tayefeh et al. 2007). This effect results from the very high affinity of the negative charges to coordinate K^+ ions which—once bound—block further entrance or exit of other ions through the mouth. In this case, no positively charged salt bridge partner is close enough in order to compete successfully with direct K^+ coordination.

In summary, a gradual loss of the probability to form salt bridges between the negatively charged C-terminus and nearby positive groups appears to be correlated with gradually reduced activity. Lower activity can be interpreted microscopically, on one hand based on the geometric effect of a smaller mouth diameter, on the other hand based on the salt bridge-induced modulation of the complex formation tendency between C-terminus and K^+ ions.

Test of the hypothesis

The computational analysis predicts that truncation of the N-terminus beyond a critical threshold corrupts channel function, because it prevents the formation of salt bridges at the cytoplasmic side of the channel protein. To test this prediction, we constructed a number of mutants in which critical amino acids, which serve as potential partners for salt bridges, were modified.

The amino acids in question on the N-terminal side are Lys^6 and Arg^{10}, which can interact with the negative charge at the C-terminus of the same or adjacent monomer. Also Glu^{12} is relevant, because it can interact with the positive charges of the N-terminus on flanking monomers. The salt bridge partner on the C-terminal side is either the carboxyl

end of Leu^{94} in the wt channel or Glu^{95} in the linker between Kcv and GFP in the chimera.

To test the significance of these charges for channel function they were mutated individually or as pairs. The impact of the mutations was tested by expressing the mutants as chimeras with GFP in HEK293 cells or by expressing the untagged protein in yeast.

The data largely support the expected importance of the salt bridges for channel function. The hypothesis predicts that a neutralisation of Glu^{95} prevents salt bridge formation. The experimental results reveal that a mutation E95Q, e.g. a neutralisation of the charge, greatly reduces the fractional detection of the channel in HEK293 cells (Fig. 4f).

Also mutations on the N-terminal side support the functional role of a salt bridge in that a modification of the pattern of positive charges in this domain results in non-functional channels. The results of monitoring fractional detection of Kcv and its mutants in a chimera with GFP in HEK293 cells are shown in Fig. 4f. The data illustrate that not only neutralisation of Arg^{10} in the mutants R10A and K6A/R10A but also charge inversion (R10D) results in non-functional channels (Fig. 4d, f). Preliminary measurements show that a neutralisation of the negative charge Glu^{12} on the other hand seems not to be crucial, because two HEK293 cells transformed with Kcv-E12A:GFP exhibited typical Kcv-type currents (data not shown).

The importance of positive charges in the N-terminal domain for function is, in principle, also supported by the yeast rescue experiments, even though the results of these experiments are not identical to those obtained in the HEK cell system. The data in Fig. 5 show that single mutations K6A and R10A are still able to rescue yeast growth at low concentrations, although growth of these cells at 0.5 mM K^+ is retarded compared to that in cells with Kcv-wt. In line with the hypothesis we find that neutralisation of both positive charges K6A/R10A fails to rescue the mutants.

Collectively the results of these experiments show that various eliminations of potential salt bridge partners reduce the likelihood for recording Kcv-channel activity in different expression systems. Individual mutations do not completely abolish channel function; they merely reduce more or less severely the likelihood of detecting functional channels (Figs. 4, 5; Gazzarrini et al. 2002). In line with the results form MD simulations the best explanation for these data is that the protein has several potential salt bridge partners in the respective domains. For this reason, it can still produce currents irrespective of mutations of critical amino acids. In this case other amino acids can provide alternative salt bridge partners. The fact that point mutations of critical amino acids impair Kcv activity in a variable manner in different expression systems suggests a role of the micro-environment on channel function. For example, different types of membranes could bias the propensity towards different salt bridge partners. This interpretation is consistent with the fact that Kcv wild-type has different functional properties depending on the expression system (Moroni et al. 2002; Gazzarrini et al. 2002; Pagliuca et al. 2007) and that an extension of TM1 dramatically alters channel function (Hertel et al. 2006).

Conclusion

The viral channel Kcv has an overall architecture, which is similar to the bacterial channels KcsA and KirBac as well as to eukaryotic Kir channels (Kuo et al. 2003; Cortes et al. 2001; Nishida et al. 2007). This includes a helical domain upstream of TM1, which was termed "slide helix" in KirBac1.1 (Kuo et al. 2003). Thus it occurs as if the slide helix is common to 2TM K^+ channels.

Previous investigations have already suggested a functional importance of this slide helix-equivalent of Kcv. Full deletion or modifications in the linker of this domain to TM1 severely affects channel activity (Moroni et al. 2002; Hertel et al. 2006). It is worth noting that a similar dependency on the N-terminal domain for function is also true for KcsA. Removal of the first 20 amino acids, i.e. the region roughly corresponding to the portion truncated in Kcv, renders the channel inactive (Cortes et al. 2001).

The present data provide insight into the function of the slide helix-equivalent in Kcv; they highlight the importance of charged amino acids in this domain, which are able to form intra- and inter-subunit salt bridges with the downstream part of TM2. The slide-helix of Kcv can be shortened by seven amino acids without compromising channel activity; it also tolerates mutations, which do not change the charge patterns. This means that neither size nor the precise architecture of this domain is crucial for function. The main structural feature of the N-terminus is the charge distribution of this domain. The computational and the experimental data are consistent with the hypothesis that positive charges in the N-terminus are forming a salt bridge with the negative charge of the carboxyl group of the C-terminus. The comparison of simulations of the wild type channel and truncated mutants suggests that these bridges and their dynamics are important for the exchange of ions between cavity and cytosolic solution. Ion transport through the cytoplasmic mouth is mediated by the negative charges at the entrance to the cavity. K^+ ions can be coordinated to these negative charges. Only if salt bridges between C-terminal negative charges and the N-terminal positive residues can be formed, K^+ can be released from its site and participate in the ion flux through the channel protein (see also Tayefeh et al. 2007).

The present data are in accord with the view that an inter-subunit interaction of the two TM domains at the

cytoplasmic boundary are of general importance in K^+ channel gating. A recent study reports the crystal structures of the open and closed state of the NaK channel (Alam and Jiang 2009). This channel has the same overall structure of 2TM K^+ channels; the structural data imply that the channel undergoes a concerted conformational change of both transmembrane domains in the course of an open/close transition. A salt bridge in NaK in a position equivalent to that in Kcv (Tayefeh et al. 2007) might be involved in this concerted motion. Also the gating motion of the TM in some Kir channels is controlled by an inter-subunit interaction between TM1 and TM2 at the helix-bundle crossing. In the case of the Kir channels, inter-subunit communication is due to H bonds (Rapedius et al. 2007a, b). In Kir channels, which are capable of H bonds, these interactions determine pH sensitivity as well as PIP_2 gating kinetics. Apart from local effects at the cytoplasmic boundary the same H bonds also affect a K^+-dependent inactivation process at the selectivity filter over a long distance (Rapedius et al. 2007a).

Acknowledgments This work was supported in part by the Deutsche Forschungsgemeinschaft (to G. T. and S. M. K), GrK1114 (to G.T.), Fonds der Chemischen Industrie (to S. M. K.) the Adolf-Messer-Stiftung (to S. M. K.) and the European Drug Initiative on Channels and Transporters (EDICT) project EU FP7 (201924) to A.M. We are grateful to D. Herten and P. Heinlein for help with microscopy (Bioquant, Heidelberg). Computer time was provided on IBM Regatta systems at the Hochschulrechenzentrum Darmstadt and at the Forschungszentrum Jülich. Yeast strains were generously provided by Dr. D. Minor (UCSF).

References

Alam A, Jiang Y (2009) High-resolution structure of the open NaK channel. Nat Struct Mol Biol 16:30–34. doi:10.1038/nsmb.1531

Anderson JA, Huprikar SS, Kochian LV, Lucas WJ, Gaber RF (1992) Functional expression of a probable *Arabidopsis thaliana* potassium channel in *Saccharomyces cerevisiae*. Proc Natl Acad Sci USA 89:3736–3740. doi:10.1073/pnas.89.9.3736

Balss J, Mehmel M, Baumeister D, Hertel B, Delaroque N, Chatelain FC, Minor DJ, VanEtten JL, Moroni A, Thiel G (2008) Transmembrane domain length of viral K^+ channels is a signal for mitochondria targeting. Proc Natl Acad Sci USA 105:12313–12318. doi:10.1073/pnas.0805709105

Beckstein O, Biggin PC, Bond P, Bright JN, Domen C, Grottesi A, Holyoake J, Sansom MSP (2003) Ion channel gating: insight via molecular simulations. FEBS 555:85–90. doi:10.1016/S0014-5793(03)01151-7

Beglov D, Roux B (1997) An integral equation to describe the solvation of polar molecules in liquid water. J Phys Chem B 101:7821–7826. doi:10.1021/jp971083h

Bolte S, Cordelières FP (2007) A guided tour into subcellular colocalization analysis in light microscopy. J Microsc 224:213–232. doi:10.1111/j.1365-2818.2006.01706.x

Brickmann J, Goetze T, Heiden W, Moeckel G, Reiling S, Vollhardt H, Zachmann C-D (1995) Interactive visualization of molecular scenarios with MOLCAD/SYBYL. In: Bowie JE (ed) Data visualisation in molecular science: tools for insight and innovation. Addison-Wesley, Reading, pp 83–97

Cordero-Morales JF, Jogini V, Lewis A, Vásquez V, Cortes DM, Roux B, Perozo E (2007) Molecular driving forces determining potassium channel slow inactivation. Nat Struct Mol Biol 14:1062–1069. doi:10.1038/nsmb1309

Cortes DM, Cuello LG, Perozo E (2001) Molecular architecture of full-length KcsA: role of cytoplasmic domains in ion permeation and activation gating. J Gen Physiol 117:165–180. doi:10.1085/jgp.117.2.165

Craven K, Zagotta WN (2004) Salt bridges and gating in the COOH-terminal region of HCN2 and CNGA1 channels. J Gen Physiol 124:663–677. doi:10.1085/jgp.200409178

Domene C, Bond PJ, Sansom MSP (2003) Membrane protein simulations: ion channels and bacterial outer membrane proteins. Adv Protein Chem 66:159–193. doi:10.1016/S0065-3233(03)66005-5

Doyle DA, Cabral JM, Pfuetzner RA, Kuo A, Gulbis JM, Cohen SL, Chait BT, MacKinnon R (1998) The structure of the potassium channel: molecular basis of K^+ conduction and selectivity. Science 280:69–76. doi:10.1126/science.280.5360.69

Essmann U, Perera L, Berkowitz ML, Darden T, Lee H, Pedersen LG (1995) A smooth particle mesh Ewald method. J Chem Phys 103:8577–8593. doi:10.1063/1.470117

Gazzarrini S, Van Etten JL, DiFrancesco D, Thiel G, Moroni A (2002) Voltage dependence of virus-encoded miniature K^+ channel Kcv. J Membr Biol 187:15–25. doi:10.1007/s00232-001-0147-5

Gazzarrini S, Kang M, Van Etten JL, Tayefeh S, Kast SM, DiFrancesco D, Thiel G, Moroni A (2004) Long-distance interactions within the potassium channel pore are revealed by molecular diversity of viral proteins. J Biol Chem 279:28443–28449. doi:10.1074/jbc.M401184200

Hamill OP, Marty A, Neher E, Sakmann B, Sigworth FJ (1981) Improved patch-clamp techniques for high-resolution current recording from cells and cell-free membrane patches. Pflugers Arch 391:85–100. doi:10.1007/BF00656997

Hertel B, Tayefeh S, Mehmel M, Kast SM, Van Etten J, Moroni A, Thiel G (2006) Elongation of outer transmembrane domain alters function of miniature K^+ channel Kcv. J Membr Biol 210:21–29. doi:10.1007/s00232-005-7026-4

Hille B (1992) Ionic channels of excitable membranes. Sinauer, Sunderland

Hong H, Szabo G, Tamm LK (2006) Electrostatic couplings in OmpA ion-channel gating suggests mechanism for pore opening. Nat Chem Biol 2:627–635. doi:10.1038/nchembio827

Humphrey W, Dalke A, Schulten K (1996) VMD—visual molecular dynamics. J Mol Graph 14:33–38. doi:10.1016/0263-7855(96)00018-5

Jiang Y, Lee A, Chen J, Cadene M, Chait BT, MacKinnon R (2002) The open pore conformation of potassium channels. Nature 417:523–526. doi:10.1038/417523a

Kale L, Skeel R, Bhandarkar M, Brunner R, Gursoy A, Krawetz N, Phillips J, Shinozaki A, Varadarajan K, Schulten K (1999) NAMD2: greater scalability for parallel molecular dynamics. J Comput Phys 151:283–312. doi:10.1006/jcph.1999.6201

Khalili-Araghi F, Tajkhorshid E, Schulten K (2006) Dynamics of K + ion conductance through Kv1.2. Biophys J 91:72–74. doi:10.1529/biophysj.106.091926

Kovalenko A, Hirata F (1998) Three-dimensional density profiles of water in contact with a solute of arbitrary shape: a RISM approach. Chem Phys Lett 290:237–244. doi:10.1016/S0009-2614(98)00471-0

Kuo A, Gulbis JM, Antcliff JF, Rahman T, Lowe ED, Zimmer J, Cuthbertson J, Ashcroft FM, Ezaki T, Doyle DA (2003) Crystal structure of the potassium channel KirBac1.1 in the closed state. Science 300:1922–1926. doi:10.1126/science.1085028

MacKerell AD Jr, Bashford D, Bellott M, Dunbrack RL, Evanseck JD, Field MJ, Fischer S, Gao J, Guo H, Ha S, Joseph-McCarthy D, Kuchnir L, Kuczera K, Lau FTK F, Mattos C, Michnick S, Ngo T, Nguyen DT, Prodhom B, Reiher WE, Roux B, Schlenkrich M, Smith JC, Stote R, Straub J, Watanabe M, Wiorkiewicz-Kuczera J, Yin D, Karplus M (1998) All-atom empirical potential for molecular modelling and dynamics. Studies of proteins. J Phys Chem B 102:3586–3616. doi:10.1021/jp973084f

MacKinnon R (2003) Potassium channels. FEBS Lett 555:62–65. doi:10.1016/S0014-5793(03)01104-9

Marti-Renom MA, Stuart A, Fiser A, Sánchez R, Melo F, Sali A (2000) Comparative protein structure modeling of genes and genomes. Annu Rev Biophys Biomol Struct 29:291–325. doi:10.1146/annurev.biophys.29.1.291

Moroni A, Thiel G (2006) Flip-flopping salt bridges gate an ion channel. Nat Chem Biol 2:572–573. doi:10.1038/nchembio1106-572

Moroni A, Viscomi C, Sangiorgio V, Pagliuca C, Meckel T, Horvath F, Gazzarrini S, Valbuzzi P, Van Etten JL, DiFrancesco D, Thiel G (2002) The short N-terminus is required for functional expression of the virus-encoded miniature K^+ channel Kcv. FEBS Lett 530:65–69. doi:10.1016/S0014-5793(02)03397-5

Nishida M, Cadene M, Chait BT, MacKinnon R (2007) Crystal structure of a Kir3.1-prokaryotic Kir channel chimera. EMBO J 26:4005–4015. doi:10.1038/sj.emboj.7601828

Pagliuca C, Goetze TA, Wagner R, Thiel G, Moroni A, Parcej D (2007) Molecular properties of Kcv, a viral-encoded K^+ channel. Biochem 46:1079–1090. doi:10.1021/bi061530w

Plugge B, Gazzarrini S, Nelson M, Cerana R, Van Etten JL, Derst C, DiFrancesco D, Moroni A, Thiel G (2000) A potassium channel protein encoded by chlorella virus PBCV-1. Science 287:1641–1644. doi:10.1126/science.287.5458.1641

Rapedius M, Fowler PW, Shang L, Sansom MSP, Tucker SJ, Baukrowitz T (2007a) H Bonding at the helix-bundle crossing controls gating in Kir. Neurone 16:602–614. doi:10.1016/j.neuron.2007.07.026

Rapedius M, Payner JJ, Payneter, Fowler PW, Shang L, Sansom MSP (2007b) Control of pH and PIP_2 gating in heteromeric Kir4.1/Kir5.1 channels by H-bonding at the helix bundle crossing. Channels 1:327–330

Roux B, Schulten K (2004) Computational studies of membrane channels. Structure 12:1343–1351. doi:10.1016/j.str.2004.06.013

Roux B, Allen T, Bernéche S, Im W (2004) Theoretical and computational models of biological ion channels. Q Rev Biophys 37:15–103. doi:10.1017/S0033583504003968

Schlenkrich M, Brickmann J, MacKerell AD Jr, Karplus M (1996) An empirical potential energy function for phospholipids: criteria for parameter optimization and applications. In: Merz KM, Roux B (eds) Biological membranes: a molecular perspective from computation and experiment. Birkhäuser, Boston, pp 31–81

Shi N, Ye S, Alam A, Chen LP, Jiang YX (2006) Atomic structure of a Na^+- and K^+-conducting channel. Nature 440:570–574. doi:10.1038/nature04508

Tayefeh S, Kloss T, Thiel G, Hertel B, Moroni A, Kast SM (2007) Molecular dynamics simulation study of the cytosolic mouth in Kcv-type potassium channels. Biochem 46:4826–4839. doi:10.1021/bi602468r

Tayefeh S, Kloss T, Kreim M, Gebhardt M, Baumeister D, Hertel B, Richter C, Schwalbe H, Moroni A, Thiel G, Kast SM (2009) Model development for the viral potassium channel. Biophys J 96:485–498. doi:10.1016/j.bpj.2008.09.050